Astron. Astrophys. 331, 821–828 (1998)

ASTRONOMY
AND
ASTROPHYSICS

The neutron star in the supernova remnant PKS 1209–52

V.E. Zavlin[1,2], **G.G. Pavlov**[2], **and J. Trümper**[1]

[1] Max-Planck-Institut für Extraterrestrische Physik, D-85740 Garching, Germany
[2] The Pennsylvania State University, 525 Davey Lab, University Park, PA 16802, USA

Received 1 September 1997 / Accepted 17 November 1997

Abstract. We re-analyzed X-ray data collected with the *ROSAT* and *ASCA* observatories on a candidate neutron star (NS) near the center of the supernova remnant PKS 1209–52. We fitted the observed spectra with NS atmosphere models. The hydrogen atmosphere fits yield more realistic parameters of the NS and the intervening hydrogen column than the traditional blackbody fit. In particular, for a NS of mass 1.4 $M_\odot$ and radius 10 km, we obtained a NS surface temperature $T_{\rm eff}$ = $(1.4 - 1.9) \times 10^6$ K and distance d = $1.6 - 3.3$ kpc versus $T = (4.2 - 4.6) \times 10^6$ K and implausibly large $d = 11 - 13$ kpc for the blackbody fit, at a 90% confidence level. Our fits suggest that the surface magnetic field is either very weak, $B \lesssim 10^{10}$ G, or it exceeds $\simeq 2 \times 10^{12}$ G. The hydrogen column density inferred from the atmosphere fits, $n_H = (0.7 - 2.2) \times 10^{21}$ cm^{-2}, agrees fairly well with independent estimates obtained from UV observations of nearby stars, radio data, and X-ray spectrum of the shell of the supernova remnant, whereas the blackbody and power-law fits give considerably lower and greater values, $n_H = (0.2 - 0.4) \times 10^{21}$ and $(5.2 - 7.0) \times 10^{21}$ cm^{-2}, respectively. The NS surface temperature inferred from the atmosphere fits is consistent with standard NS cooling models.

Key words: stars: neutron – supernovae: individual PKS 1209-52 – X-rays: stars – radiation mechanisms: thermal

1. Introduction

In addition to about 15 radio pulsars associated with supernova remnants (Gaensler & Johnston 1995), several *radio-silent* isolated neutron star (NS) candidates within supernova remnants (SNRs) have been observed with the X-ray observatories *HEAO*–1, *Einstein*, *EXOSAT*, *ROSAT*, and *ASCA* (see Caraveo et al. 1996 for a review). These objects have not been detected outside the X-ray range, and their X-ray spectra resemble blackbody (BB) spectra with temperatures of a few million kelvin. If they are indeed thermally emitting NSs, the analysis of their radiation provides an opportunity to study thermal evolution of NSs of ages $\sim 10^3 - 10^5$ yr, which is important for elucidating the properties of the superdense matter in NS interiors.

One of the most convincing examples of such objects is the point-like source 1E1207.4–5209 within the barrel-shaped radio, X-ray, and optical SNR PKS 1209–52 (also known as G269.5+10.0). From the analysis of radio and optical observations of this SNR, Roger et al. (1988) estimated its age $\sim$ 7000 yr, with an uncertainty of a factor of 3, and concluded that the remnant is in an adiabatic expansion phase. The distance to PKS 1209–52 is not well determined — estimates in the range $1.1 - 3.9$ kpc were suggested (Milne 1979; Mills 1983). Estimates of the interstellar hydrogen column density from the radio and optical data yield $n_{H,21} \equiv n_H/(10^{21}$ cm$^{-2}) \sim 1.0 - 1.8$ (see Roger et al. 1983 and Kellet et al. 1987 for references), consistent with a distance $d \sim 1 - 2$ kpc.

After the first X-ray detection of PKS 1209–52 with *HEAO*–1 (Tuohy et al. 1979), the point source 1E1207.4–5209 was discovered with the *Einstein* observatory (Helfand & Becker 1984), 6′ off-center the 81′ diameter SNR. Matsui et al. (1988) concluded that its spectrum can be interpreted as a BB spectrum with an apparent temperature $T \simeq 1.4 \times 10^6$ K (assuming $n_{H,21}$ = 3.2, as inferred from the data obtained with *HEAO*–1). The *Einstein* High Resolution Imager (HRI) observations showed a lack of diffuse X-ray emission around 1E1207.4–5209 (later confirmed by the *ROSAT* HRI observations), which greatly simplifies the analysis of the point source radiation. From the analysis of observations made with the *EXOSAT* Position Sensitive Detector, Kellett et al. (1987) estimated the BB temperature of the central object $T \simeq 1.8 \times 10^6$ K (at $n_{H,21}$ = 1.1), which implies an emitting area of a radius $(3 - 4)\ d_2$ km, where $d_2 = d/(2$ kpc). Applying the Raymond & Smith (1977) line-emission model, Kellet et al. estimated also an average SNR temperature, $\sim 1.7 \times 10^6$ K, and the hydrogen column towards the SNR, $n_{H,21} \simeq 1.4$, consistent with the values obtained from radio and optical data.

Observations of PKS 1209–52 and its central source with *ROSAT* and *ASCA* have further supported the NS hypothesis for 1E1207.4–5209. Mereghetti et al. (1996; hereafter MBC96) showed that the *ROSAT* data of 1E1207.4–5209 can be interpreted as blackbody emission of $T \simeq 3 \times 10^6$ K from an area

with radius $R \simeq 1.5\ d_2$ km. The authors noticed that this temperature is too high to be explained in the framework of a cooling NS with the age of PKS 1209–52 ($\sim 10^4$ yr). The hydrogen column inferred from the BB fit, $n_{H,21} \simeq 0.4$, is $3-4$ times lower than the estimate given by Kellett et al. (1987). From observations at 4.8 GHz, MBC96 found an upper limit of ~ 0.1 mJy on the radio flux from 1E1207.4–5209. They also set a deep limit of $V > 25$ for an optical counterpart in the *Einstein* HRI error circle, which supports the hypothesis that 1E1207.4–5209 is indeed an isolated NS.

Vasisht et al. (1997; hereafter V97) have recently analyzed *ASCA* observations of 1E1207.4–5209. They found that each of the three spectra obtained with the *ASCA* detectors can be fitted by a BB spectrum consistent with that obtained from the analysis of the *ROSAT* data. The hydrogen column is poorly restricted in the *ASCA* spectral fits due to low detector sensitivities at photon energies below 0.5 keV. Using a fit with a Raymond-Smith model at fixed cosmic abundances to the *ROSAT* data of the SNR shell, V97 estimated the remnant temperature $\sim (1.9-2.3)\times 10^6$ K and the foreground column density $n_{H,21} \simeq 0.6-0.9$. They attributed the difference in n_H between the NS and SNR fits to either separate lines of sight or the large column density that the shell X-rays can encounter in the SNR postshocked gas.

Based on the results of the blackbody analysis, both MBC96 and V97 concluded that 1E1207.4–5209 is an isolated NS with hot spots on its surface, aligned with the magnetic poles. V97 suggested that the spots are heated either by dissipative heating in the NS interior or by the bombardment of polar caps by relativistic particles from the NS magnetosphere if 1E1207.4–5209 is an active pulsar. However, the former hypothesis can hardly explain the small sizes of the hot spots, even with allowance for large anisotropy of thermal conductivity of the magnetized NS crust. The latter heating mechanism is also in doubt because of the absence of radio and γ-ray emission from 1E1207.4–5209. Moreover, both the *ROSAT* and *ASCA* data did not reveal pulsations, which may not be consistent with the presence of the hot spots unless the magnetic and rotation axes are coaligned.

Although it looks very plausible that 1E1207.4–5209 is a thermally emitting isolated NS, the BB interpretation adopted by previous authors leaves several controvertible points. Since thermal radiation emitted by NS atmospheres may significantly differ from the BB radiation, it is natural to employ more realistic models of NS radiation to resolve the inconsistencies following from the simplified BB interpretation. Here we present a *combined* analysis of the *ROSAT* and *ASCA* data based on NS atmosphere models (Pavlov et al. 1995, and references therein). These models have been applied successfully to the interpretation of the soft X-ray radiation from, e.g., the Vela pulsar (Page et al. 1996) and the brightest millisecond pulsar, J0437–4715 (Zavlin & Pavlov 1998; Pavlov & Zavlin 1997). These examples show that fitting soft X-ray pulsar spectra with hydrogen or helium atmosphere models results, as a rule, in lower effective temperatures and greater emitting areas (or smaller distances) than those obtained from the BB fits.

We show in Sect. 2 that, indeed, the model atmosphere fits of the X-ray radiation from 1E1207.4–5209 yield an NS surface temperature compatible with NS cooling models, and they do not require hot spots on the NS surface. Moreover, the hydrogen column density inferred from this interpretation is in excellent agreement with that obtained from our fits of the SNR X-ray radiation as well as with independent estimates of n_H for stars in the vicinity of 1E1207.4–5209 (Sect. 3). These results warrant application of the same approach to other similar objects and enable one to obtain reliable estimates of surface temperatures of NSs of different ages.

2. Observations and results

We used the archival *ROSAT* and *ASCA* data of 1E1207.4–5209 (see MBC96 and V97 for a detailed description). Four *ROSAT* Position Sensitive Proportional Counter (PSPC) pointings (obtained in July 1993, with exposure times about $5-6$ ks each — see Table 2 in MBC96) were centered at different positions (off-axis angles between $16'$ and $33'$). We checked that the spectra of 1E1207.4–5209 extracted from each of the four data sets and properly corrected for the PSPC response are consistent with each other. For the combined analysis with the *ASCA* data we chose the *ROSAT* PSPC observation with the minimum off-axis angle $16'$ (exposure time ~ 4.97 ks). With the aid of the MIDAS/EXSAS package (Zimmermann et al. 1994) we extracted a raw spectrum from a region with a radius $r \simeq 75''$ centered on the source and subtracted the background spectrum estimated from an annulus with the inner radius r and outer radius $\simeq 3r$. (The backgrounds for observations with other *ROSAT* and *ASCA* instruments were estimated in the same manner). The (off-axis) source count rate is 0.145 ± 0.005 s^{-1}. We binned the source spectrum in the $0.1-2.4$ keV energy range into 24 spectral bins with signal-to-noise ratios greater than 5. The *ROSAT* HRI counts for each of the three on-axis pointings (obtained in August 1992 and July 1994; total exposure time ~ 14.5 ks) were selected from the circles of $r \simeq 22''$. The corresponding source count rate is 0.064 ± 0.003 s^{-1}, in agreement with MBC96.

The *ASCA* data were obtained in July 1994, with two Solid State Imaging Spectrometers, SIS0 and SIS1, in the "2-CCD bright" mode, and two Gas Scintillation Imaging Spectrometers, GIS2 and GIS3, in the "pulse-height" mode. The SIS1 image of 1E1207.4–5209 is too close to the edge of the CCD chip for a reliable spectral analysis. To reduce the *ASCA* data, we used the FTOOLS/XSELECT software (v. 3.5). The SIS0 source counts collected in ~ 21 ks (with "high" and "medium" bit rates) were extracted from the circle of $r \simeq 4'$, the total source count rate is 0.0556 ± 0.0017 s^{-1}. The SIS0 spectrum was binned into 38 spectral bins (with minimum number of counts equal 20) in the $0.4-10.0$ keV range. The GIS2 and GIS3 source counts were extracted from circles of $r \simeq 9'$ (exposure ~ 19 ks for the high plus medium bit rates). The source count rates are 0.0425 ± 0.0018 (GIS2) and 0.0533 ± 0.0025 s^{-1} (GIS3). The spectra were binned into 39 and 46 spectral bins (with the same binning scheme as for SIS0) in the $0.2-10.0$ keV range for

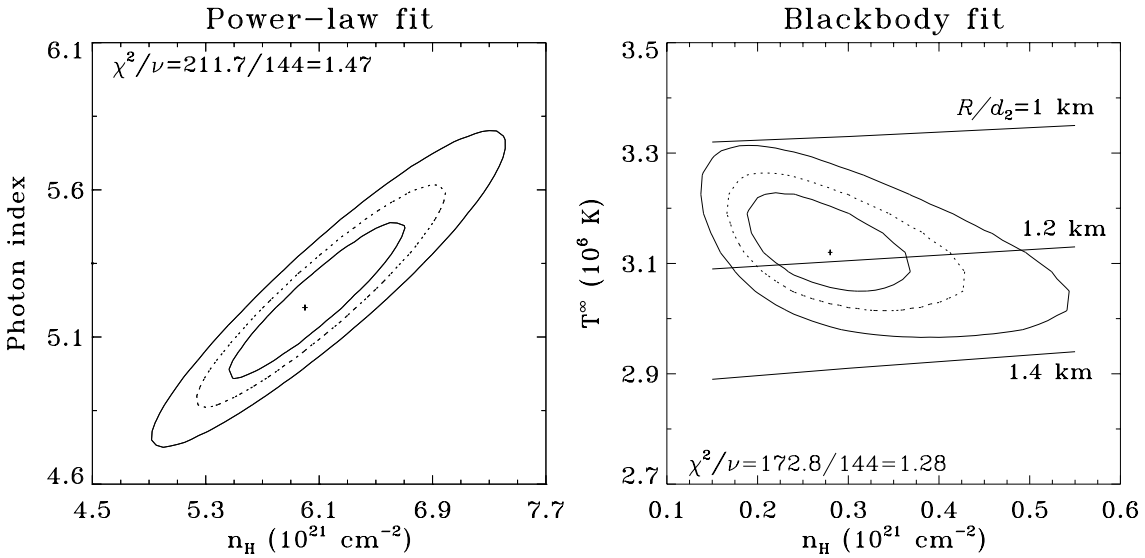

Fig. 1. 68%, 90% and 99% confidence contours ($\Delta\chi^2$ = 3.5, 6.3 and 11.3, respectively) for the power-law and blackbody simultaneous fits to the *ROSAT* PSPC and *ASCA* SIS0, GIS2 and GIS3 spectra of 1E1207.4–5209. The lines in the right panel correspond to constant values of radius of emitting area at a distance d = 2 kpc.

GIS2 and GIS3, respectively. The total source count rates for all the three *ASCA* instruments are somewhat lower than those reported by V97, perhaps because of different screening criteria we applied. The SIS0 and GIS spectral responses (redistribution matrix and ancillary response files) were created with the standard FTOOLS codes "sisrmg" and "ascaarf".

For our spectral analysis we used the XSPEC package (v. 9.01) with its standard χ^2 fitting. As a first step, we fitted the count rate spectra *simultaneously* for the four instruments, *ROSAT* PSPC and *ASCA* SIS0, GIS2, and GIS3, with the traditional power-law and BB models. Fig. 1 shows the results of these fits. The power-law fit yields a photon index $\gamma = 5.2\ (+0.4, -0.3)$ and a hydrogen column density, $n_{H,21} = 6.0\ (+1.0, -0.8)$ (minimum $\chi^2_\nu = 1.47$, $\nu = 144$; the uncertainties hereafter are at a 90% confidence level). These values of γ and n_H are better constrained than those obtained by MBC96 from the PSPC data alone, $\gamma = 3.9\ (+1.5, -1.4)$ and $n_{H,21} = 3.0\ (+2.5, -1.8)$ (minimum $\chi^2_\nu = 1.61$, $\nu = 10$). The photon index is unusually large in comparison with typical values, $\gamma \simeq 1.5 - 2.5$, observed from, e.g., X-ray emitting radio pulsars (Becker & Trümper 1997), and the hydrogen column density significantly exceeds the values obtained by independent measurements (see below). These discrepancies imply that the power-law interpretation is inadequate.

The BB temperature (as measured by a distant observer), $T^\infty = 3.12\ (+0.15, -0.11) \times 10^6$ K, the apparent radius of the emitting area, $R_a = 1.21\ (+0.10, -0.13)\ d_2$ km, and the bolometric luminosity, $L^\infty_{\rm bol} = 0.93\ (+0.19, -0.11) \times 10^{33}\ d_2^2$ erg s^{-1}, obtained from the combined fit (Fig. 1) are very close to the values from the separate fits of the *ROSAT* and *ASCA* data by MBC96 and V97. The hydrogen column density in the combined fit, $n_{H,21} = 0.28\ (+0.15, -0.12)$, is compatible with $n_{H,21} = 0.3 - 0.5$ inferred from the separate *ROSAT* PSPC spectrum. Although the quality of the BB fit is better than the quality of the power law fit, the n_H values look surprisingly low in comparison with the $(1.0 - 1.8) \times 10^{21}$ cm^{-2} obtained from independent estimates (see Sect. 1).

Since thermal NS spectra, as well as spectra of ordinary stars, cannot exactly coincide with the BB spectra because of the effects of radiative transfer in the emitting layers, it is natural to compare them with more realistic model spectra of NS atmospheres (e.g., Pavlov et al. 1995). Strongest deviations from the BB spectrum are expected if the NS surface is covered with a hydrogen atmosphere. Hydrogen may appear at the NS surface as a result of, e.g., accretion of interstellar matter or post-supernova accretion of a fraction of the ejected envelope. Due to the huge surface gravity (typical gravitational acceleration $\sim 10^{14} - 10^{15}$ cm s^{-2}), heavier chemical elements sink down in deeper layers and do not affect the properties of emitted radiation, whereas hydrogen remains at the surface. The shape of the spectrum emitted by an atmosphere depends on the strength B of the NS surface magnetic field. The lack of pulsations does not allow one to estimate B using the pulsation period and its derivative, as is usually done for pulsars. The absence of statistically reliable features in the observed spectra (see Fig. 2), which could be associated with an electron cyclotron line at $E_{Be} = 11.6(B/10^{12}$ G) keV, prevents one to make a direct estimation of B. Therefore, one has to try the atmosphere models with both low ($B \lesssim 10^{10}$ G) and high magnetic fields. (In the former case, the field does not affect the properties of emergent radiation [Zavlin et al. 1996], so that we can merely put $B = 0$). In the case of strong nonuniform field ($B \gtrsim 10^{12}$ G), the NS should have a nonuniform temperature distribution along its surface because of the high anisotropic thermal conductivity in the NS crust (e.g., Shibanov & Yakovlev 1996). However, since we have no information about the field geometry, we assume that

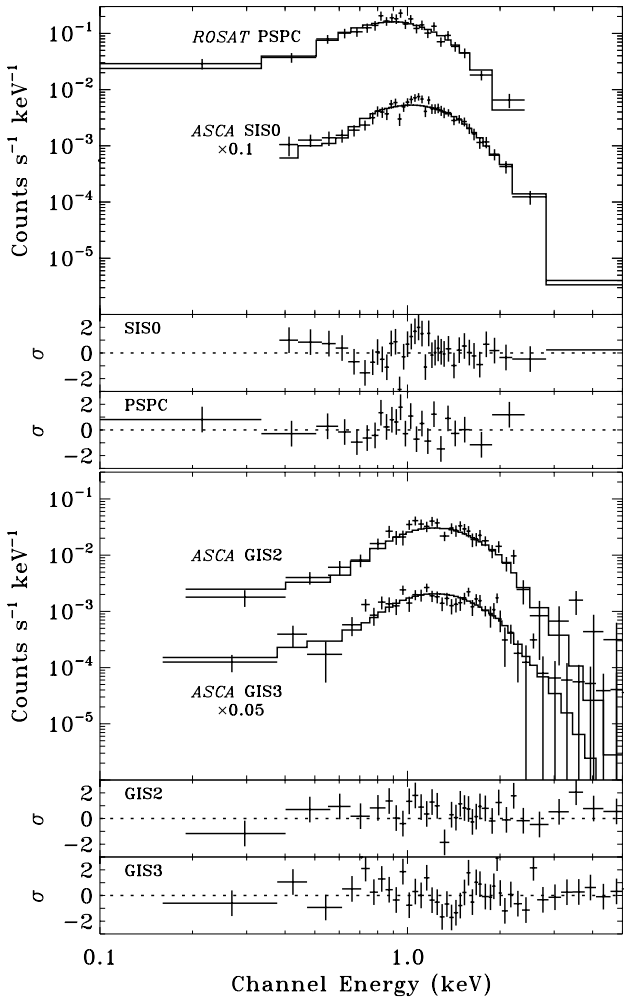

Fig. 2. Count rate spectra observed from 1E1207.4–5209, together with the best-fit hydrogen atmosphere model spectra for $B = 10^{13}$ G (cf. Fig. 3). The residuals (in units of σ) are shown separately for the four instruments. The spectra of SIS0 and GIS3 are reduced for clarity by factors of 10 and 20, respectively.

the magnetic field has the same strength and is directed radially everywhere at the surface, and that the effective temperature is uniform. This assumption reduces the number of fitting parameters and can be considered as a reasonable first approximation for investigating the atmosphere effects.

Fig. 3 shows results of fits of the combined *ROSAT* and *ASCA* data with hydrogen atmosphere models for three fixed values of the magnetic field. In these fits we assume canonical values for the NS mass and radius, $M = 1.4\ M_\odot$ and $R = 10$ km, and consider the distance as a fitting parameter. The models with $B = 0$ (left panels) and 10^{13} G (right panels) result in close values of the distance, effective temperature at the NS surface and bolometric luminosity, $d = 2.3\ (+1.0, -0.7)$ kpc, $T_{\rm eff} = 1.63\ (+0.27, -0.19) \times 10^6$ K, $L_{\rm bol} = 5.0\ (+4.3, -1.8) \times 10^{33}$ erg s^{-1}, and $d = 2.3\ (+1.0, -0.8)$ kpc, $T_{\rm eff} = 1.65\ (+0.20, -0.17) \times 10^6$ K, $L_{\rm bol} = 5.3\ (+3.0, -2.0) \times 10^{33}$ erg s^{-1}, for $B = 0$ and 10^{13} G, respectively. Since the nonmagnetic spectra are softer at lower energies, the hydrogen column density at $B = 0$, $n_{H,21} = 1.0\ (+0.5, -0.6)$, is lower than for the strong magnetic field, $n_{H,21} = 1.5\ (+0.7, -0.6)$. We checked that folding the models within the 90% confidence region with the *ROSAT* HRI response yields count rates compatible with those observed. When the field strength varies in the range $5 \times 10^{12} \lesssim B \lesssim 5 \times 10^{13}$ G, the fitting parameters remain approximately the same because the model spectra are almost insensitive to the B value in the corresponding domain of energies and effective temperatures. When B exceeds $\sim 5 \times 10^{13}$ G, the proton cyclotron line centered at $E_{Bp} = 0.063(B/10^{13}\ {\rm G})$ keV (cf. Bezchastnov et al. 1996) enters the SIS energy range, which makes the fits statistically unacceptable. (This line moves above ~ 5 keV, the maximum energy where the NS flux is still above the background [Fig. 2], at superstrong magnetic fields, $B \gtrsim 8 \times 10^{14}\ G$, for which the models we used here are not directly applicable.) When B falls below $\sim 5 \times 10^{12}$ G, the low-energy wing of the electron cyclotron line gets into the *ASCA* range, and the model spectra become softer at $E \gtrsim 2$ keV. As a result, the confidence contours in the n_H-d and n_H-$T_{\rm eff}$ planes move to greater d and $T_{\rm eff}$, and lower n_H, towards the BB contours. An example is shown in the middle panels of Fig. 2 for $B = 2 \times 10^{12}$ G, for which the best-fit distance is about 50% larger than at $B = 10^{13}$ G. When the field is lower than $\sim 5 \times 10^{11}$ G, but greater than $\sim 1 \times 10^{10}$ G, the atmosphere model fits become statistically unacceptable because the core of the electron cyclotron line gets into the *ASCA*/*ROSAT* range.

The atmosphere models depend not only on B, but also on the NS mass and radius which determine the gravitational acceleration (one of our model parameters) and the gravitational redshift factor $g_r = (1 - 0.295 M_*/R_{10})^{1/2}$, where $M_* = M/M_\odot$, $R_{10} = R/10$ km. To illustrate this effect, we present in Fig. 4 the best-fit parameters at $B = 10^{13}$ G in a wide range of R and M allowed by equations of state of the NS matter. Although the effective temperature at the NS surface, $T_{\rm eff}$, varies by about $\pm 20\%$ in the allowed R-M domain, the apparent effective temperature (as measured by a distant observer), $T_{\rm eff}^\infty = g_r T_{\rm eff}$, remains almost constant, $(1.23 - 1.31) \times 10^6$ K, because the redshift is compensated by the change of the unredshifted NS spectrum (it softens in the Wien tail with increasing M and decreasing R at given $T_{\rm eff}$). Owing to the approximate constancy of $T_{\rm eff}^\infty$, the apparent and "true" bolometric luminosities depend on R and M as $L_{\rm bol}^\infty \propto R_\infty^2 = R^2/g_r^2$ and $L_{\rm bol} = g_r^{-2} L_{\rm bol}^\infty \propto R^2/g_r^4$. The latter dependence explains the non-monotonous behavior of $L_{\rm bol}$ at higher M. The best-fit d and n_H are almost independent of M at higher R, when g_r is close to 1. At lower R the variations are stronger, albeit within the statistical uncertainties of these parameters (cf. Fig. 2). The distance inferred at assumed R and M can be approximately described, in the allowed mass-radius domain, by a linear equation: $d = 0.5 M_* - 0.4 + (2.5 - 0.3 M_*) R_{10}$ (in kpc); it grows with R faster than for the BB interpretation. Notice that if d is determined more accurately in future observations of the SNR and its central source, this equation would delimit a band in the M-R plane constraining equation of state of the NS matter.

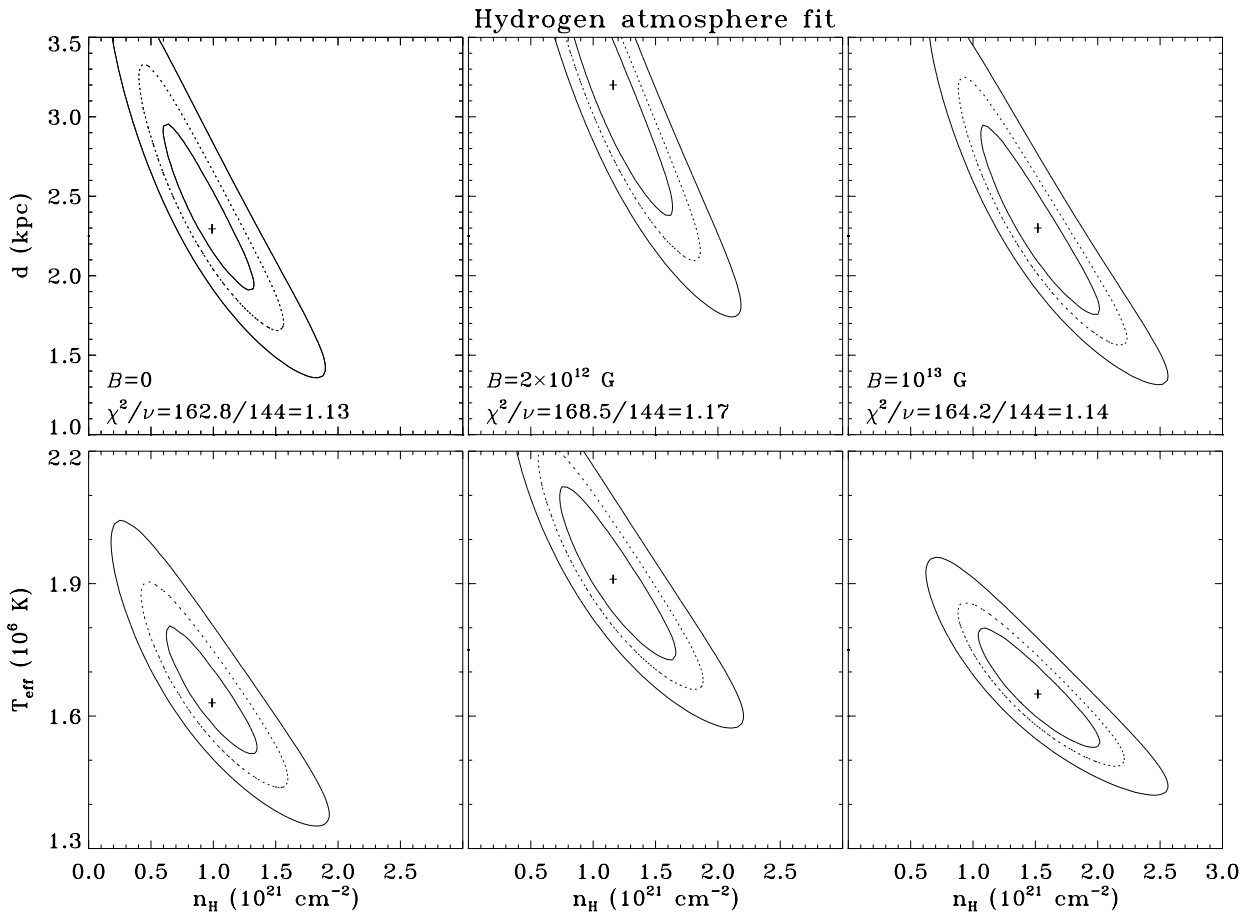

Fig. 3. 68%, 90% and 99% confidence contours for the NS hydrogen atmosphere fits to the the combined $ROSAT$ and $ASCA$ data for M = 1.4 $M_\odot$, R = 10 km, and three values of the surface magnetic field B.

Since the hydrogen atmosphere fits yield n_H greater than the BB fit by a factor of $3-5$, it is important to estimate this parameter independently. For this purpose, we fitted the SNR emission with various models for thermal plasma radiation. We extracted the SNR spectrum from a bright region of the $ROSAT$ PSPC image of the remnant shell within the $r \simeq 5'$ circle centered at $\alpha_{(2000)} = 12^{\rm h}11^{\rm m}56\overset{\rm s}{.}0$, $\delta_{(2000)} = -52^\circ36'36''$. Three models available with the XSPEC package, "vraymond", "vmeka", and "vmekal" (Raymond-Smith, Mewe-Gronenschild-Kaastra, and Mewe-Kaastra-Liedahl models with variable abundances) give satisfactory fits ($\chi^2_\nu < 1.0$) with the column density to the SNR in the range of $(1.1-1.9)\times10^{21}$ cm^{-2}, consistent with the hydrogen atmosphere fits of 1E1207.4–5209, but certainly in excess of the BB fits. The inferred plasma temperature is $(1.9-2.1)\times10^6$ K. These results were obtained with a moderate excess of abundances of Al and Si whose emission lines are prominent in the SIS spectra of the SNR shell. Abundances of other elements are close to standard values. The SNR parameters inferred from our fits are consistent with those obtained by Kellett et al. (1987) from the $EXOSAT$ data. The lower hydrogen density, $n_{H,21} = 0.6-0.9$, obtained by V97, is likely associated with fixed cosmic abundances adopted, which resulted in lower statistical quality of their fits ($\chi^2_\nu = 1.8$). Note, however, that the emission models we and V97 used assume a single-temperature plasma in collisional ionization equilibrium. Both the temperature nonuniformity and nonequilibrium ionization may significantly affect the SNR X-ray emission (see, e.g., Bocchino et al. 1997, and references therein), so that the inferred SNR parameters, particularly the element abundances and temperature, may not be very accurate.

3. Discussion and conclusions

We have shown that the X-ray spectra of the isolated NS 1E1207.4–5209 in the center of the SNR PKS 1209–52 observed with the $ROSAT$ PSPC and HRI and $ASCA$ SIS0, GIS2 and GIS3 can be interpreted as *thermal radiation from the hydrogen-covered, uniformly heated surface of the NS*. The proposed interpretation resolves all the inconsistencies which follow from the BB interpretation of radiation of this object.

First, the range of distances, $d = 1.5-3.2$ kpc, inferred for the standard NS mass $M = 1.4M_\odot$ and radius R = 10 km, is within the (conservative) limits, $1.1-3.9$ kpc, obtained from radio observations of the SNR. This range shifts to lower distances with decreasing R and M: e.g., $d = 1.2-2.6$ kpc for

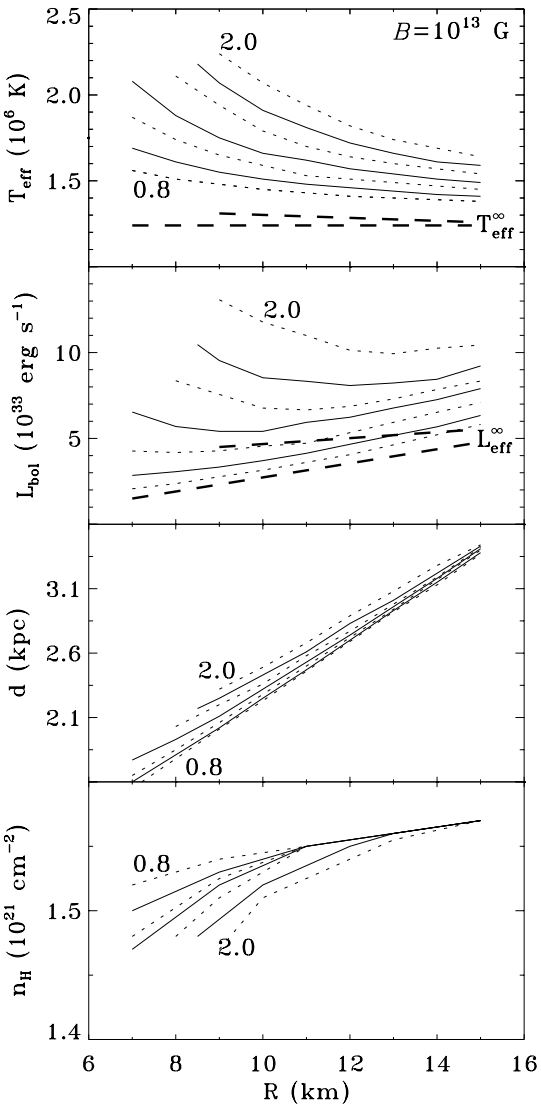

Fig. 4. Dependences of the best-fit parameters for the atmosphere fits on the NS radius R at different values of the NS mass, $M/M_\odot$ = 0.8, 1.0, ... 2.0. The thick dashed lines delimit the ranges of the apparent temperature and luminosity (upper and lower dashed curves correspond to $M/M_\odot$ = 2.0 and 0.8, respectively).

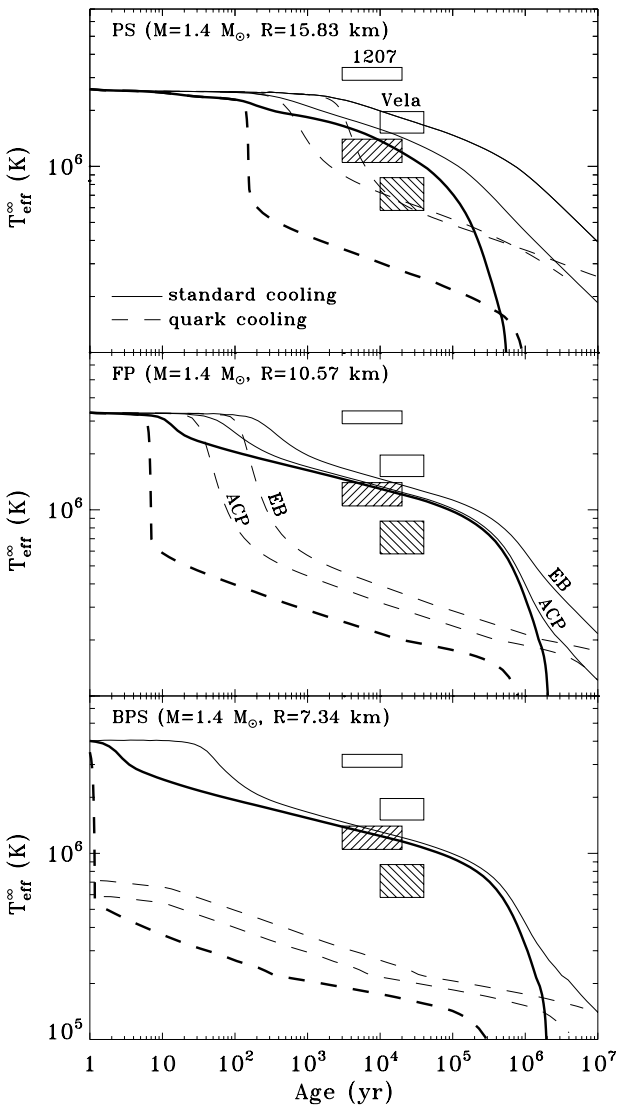

Fig. 5. Comparison of the surface temperatures inferred from the BB (empty boxes) and hydrogen atmosphere (hatched boxes) fits of the spectra of 1E1207.4–5209 and the Vela pulsar with NS cooling curves for three EOS of the NS matter, two NS compositions, and different models for additional frictional heating. The cooling curves are taken from Van Riper et al. (1995), where more detailed explanations can be found.

M = 1.0 $M_\odot$, R = 8 km. Thus, the assumption about hot spots on the NS surface, which is difficult to reconcile with the lack of pulsar activity in 1E1207.4–5209, is superfluous in our model.

Second, the effective temperature $T_{\rm eff} = (1.4-1.9)\times10^6$ K ($T^\infty_{\rm eff}$ = (1.0 − 1.6) × 10^6 K), obtained from the fits with our hydrogen atmosphere models, matches well with a number of NS cooling models (see Fig. 5 and discussion below). On the contrary, it is difficult to reconcile the results of the BB interpretation with models of the NS cooling.

Third, the inferred hydrogen column density towards the 1E1207.4–5209, $n_{H,21}$ = 0.9 − 2.2 and 0.5 − 1.5 for high and low surface magnetic fields, respectively, agrees well with $n_{H,21}$ = 1.1 − 1.9 obtained from fitting the spectra of the SNR shell. These estimates are consistent with the n_H values obtained by Kellett et al. (1987) from the *EXOSAT* observations of PKS 1209–52. Moreover, measurements of n_H from UV observations of several stars in the vicinity of 1E1207.4–5209 (l = 296.5°, b = 9.9°) yield hydrogen column values in virtually the same range (Fruscione et al. 1994): $n_{H,21}$ = 1.1 − 1.5 for HD112244 (l = 303.6°, b = 6.0°, d = 1.9 kpc), $n_{H,21}$ = 1.4 for HD115842 (l = 307.1°, b = 6.8°, d = 1.9 kpc) and HD111822 (l = 303.1°, b = 10.2°, d = 2.5 kpc). On the contrary, the BB fit gives $n_{H,21}$ = 0.15 − 0.45, clearly incompatible with all the other independent estimates.

The fact that 1E1207.4–5209 shows no pulsar activity can be explained, in addition to the trivial explanation of unfavorable

orientation of its magnetic and rotational axes, by slow rotation or/and low magnetic field of the NS, so that it falls below the "death line" on the P-$\dot{P}$ diagram, $\dot{P}/P^3 = 2 \times 10^{-17}$ s^{-3}. For the simplest model of the magnetic dipole radiator, the pulsar period increases with time t as $P = (P_0^2 + 2t_0 t)^{1/2}$, where $t_0 = (8\pi^2/3)(B^2R^6/Ic^3) = 0.97 \times 10^{-13} B_{13}^2 R_{10}^6 I_{45}^{-1}$ s, $I = 10^{45} I_{45}$ g cm^2 is the moment of inertia of the NS and $B_{13} = B/(10^{13}$ G). The condition that the NS is below the death line can be written as $t_0/P^4 < 2 \times 10^{-17}$ s^{-3}, or $P > 8.4 B_{13}^{1/2} R_{10}^{3/2} I_{45}^{-1/4}$ s. Hence, if B is in the range of strong magnetic fields allowed by our fits, $0.2 \lesssim B_{13} \lesssim 8$, we may expect that the NS rotates slowly, $P \gtrsim 1 - 2$ s. If faster pulsations are discovered in future X-ray observations of 1E1207.4–5209, it would indicate that B is in the other range compatible with our fits: $B \lesssim 10^{10}$ G. It is worth noting that if the NS was born as a pulsar at an appreciable distance from the death line, only an enormous magnetic field, $B \gtrsim 5 \times 10^{15}$ G at standard NS parameters, could decelerate its rotation so that the pulsar would "die" at the relatively young age, $t \sim 10^4$ yr. Hence, discovery of slow pulsations would mean that the NS was born slowly rotating unless its magnetic field is superstrong.

Since we have estimated the effective temperature of the NS, it is interesting to compare it with what is predicted by various cooling models. Fig. 5 shows examples of NS cooling curves from Van Riper et al. (1995) for three equations of state (EOS), stiff (Pandharipande–Smith [PS]), intermediate (Friedman–Pandharipande [FP]) and soft (Baym–Pethick–Sutherland [BPS]), and two interior compositions resulting in slow and fast cooling (solid and dashed lines, respectively). Cooling curves without additional heating are depicted by thick lines, whereas thin lines show cooling curves for two models, proposed by Epstein & Baym (EB) and Alpar, Cheng & Pines (ACP), for pinning of the superfluid vortices to the crust lattice (see Van Riper et al. 1995 for references and detailed explanations). They correspond to strong and weak frictional heating associated with the dissipation of energy of differential rotation between the NS crust and superfluid interior (only the EB model is available for the BPS EOS). In the same picture we plot boxes corresponding to the inferred atmosphere and BB temperatures of 1E1207.4–5209, assuming its age in the range $(0.3 - 2) \times 10^4$ yr, and similar boxes for the Vela pulsar whose X-ray radiation was investigated in terms of the hydrogen atmosphere models by Page et al. (1996). We adopted $(1-4) \times 10^4$ yr for the Vela age, between the conventional characteristic age $P/2\dot{P}$ and an upper limit estimated by Lyne et al. (1996). We see that the BB temperature of 1E1207.4–5209 is well above the values predicted by all these cooling models, whereas the BB temperature of the Vela pulsar is compatible only with the standard (slow) cooling model supplemented by strong heating for the stiff EOS. The effective temperature of 1E1207.4–5209 obtained with the atmosphere fits is compatible, given the poorly known age, with the slow cooling models for all the three EOS, at moderate or no heating. For the stiff EOS, it is also compatible with the fast (quark) cooling accompanied by strong frictional heating. However, the large NS radius for this EOS would mean a distance $d \simeq 2.5 - 5.2$ kpc (cf. Fig. 4), uncomfortably large in comparison with conventional estimates. The same cooling curve (fast cooling with the EB heating for the stiff EOS) is the only one which goes through both the 1E1207.4–5209 and Vela pulsar boxes obtained from the atmosphere fits. This, however, does not necessarily mean that slow cooling models or other EOS or other heating rates are excluded. First, the *ROSAT* PSPC spectrum of the Vela pulsar, used in both BB and atmosphere fits, was not observed directly because the pulsar was not resolved from a surrounding minebula of $2'$ diameter, which makes the results of the spectral fits less certain. Second, one cannot exclude, in principle, that the NS of the Vela pulsar differs from 1E1207.4–5209 (e.g., the mass of the former may be greater, that could lead to an "exotic" interior composition associated with an enhanced neutrino luminosity and accelerated cooling). Finally, there exist many more cooling models than shown in Fig. 5, and some of them may satisfy both the 1E1207.4–5209 and Vela pulsar temperatures. For instance, a strong neutrino emission induced by the nucleon Cooper pair formation process (see Page 1997, and references therein), which was neglected in most of the previous NS cooling models, may result in great variety of cooling curves, depending on the (unknown) parameters of the nucleon pairing (Yakovlev 1997, private communication). For a more detailed comparison of the inferred temperatures with the cooling models, it would be very important to evaluate more accurately the distance to PKS 1209–52 (which would constrain the NS radius and hence the EOS) and the age of this object.

There exist a number of other radio silent isolated NS candidates whose observational manifestations are similar to those of 1E1207.4–5209. The most convincing example is 1E/RXJ0820–4247 in the SNR Puppis A, whose BB temperature, $\sim 3 \times 10^6$ K, and radius, ~ 2 km (Petre et al. 1996), virtually coincide with those of 1E1207.4–5209. Another example with similar properties is RXJ0002+6246 in the SNR G117.7+0.6 (Hailey & Craig 1995), whose identification is, however, less certain because of its faintness (likely, due to a larger distance and greater n_H). We expect that applying the NS atmosphere models to the analysis of such objects will allow us to evaluate their radii and effective temperatures, and to constrain their magnetic fields.

One more radio-silent NS candidate, 1E1613–5055 in the center of the SNR RCW 103 (Tuohy & Garmire 1980), appears as a different kind of object — the BB fit of its spectrum yields a considerably higher temperature, $\sim 7 \times 10^6$ K, at a few times smaller radius of the emitting region (Gotthelf et al. 1997). However, this object is deeply immersed in the remnant diffuse emission so that it is hard to separate its spectrum from that of the SNR, with the limited spatial resolution of *ASCA*. We expect that the forthcoming *AXAF* and *XMM* missions would resolve the point source and provide a spectrum suitable for the detailed analysis.

Acknowledgements. We are grateful to Ken Van Riper for providing us with the cooling curves in numerical form, to Dima Yakovlev for clarifying various aspects of the NS cooling, to Gordon Garmire for the discussion of X-ray observations of isolated NSs in SNRs, and to the anonymous referee whose critical remarks helped us to improve the

paper. The *ASCA* data were obtained through the High Energy Astrophysics Science Archive Research Center Online Service, provided by the NASA/Goddard Space Flight Center. The work was partially supported through NASA grant NAG5-2807, NASA ADP grant, INTAS grant 94-3834 and DFG-RBRF grant 96-02-00177G. VEZ thanks the Pennsylvania State University for hospitality and acknowledges the Max-Planck fellowship.

References

Becker W., Trümper J., 1997, A&A 326, 682
Bezchastnov V. G., Pavlov G. G., Shibanov Yu. A., Zavlin V. E., 1996, in: Kouveliotou C., Briggs M. F., Fishman G. J (eds). Proc. 3rd Huntsville GRB Symposium, AIP Conf. Proc. 384, NY, Woodbury, p. 907
Bocchino F., Maggio A., Sciortino S., 1997, ApJ 481, 872
Caraveo P. A., Bignami G. F., Trümper J., 1996, A&AR 7, 209
Fruscione A., Hawkins I., Jelinsky P., Wiercigroch A., 1994, ApJS 94, 127
Gaensler B. M., Johnston S., 1995, Proc. Astron. Soc. Australia, 12, 76
Gotthelf E. V., Petre R., Hwang U., 1997, ApJ 487, L175
Hailey C. J., Craig W. W., 1995, ApJ 455, L151
Helfand D. J., Becker R. H., 1984, Nat 307, 215
Kellett B. J., et al., 1987, MNRAS, 225 199
Lyne A. G., Pritchards R. S., Graham-Smith F., Camilo E., 1996, Nat 381, 497
Matsui Y., Long K. S., Tuohy I. R., 1988, ApJ 329, 838
Mereghetti S., Bignami G. F., Caraveo P. A., 1996, ApJ 464, 842 (MBC96)
Mills B. Y., 1983, in: Danziger J., Gorenstein P. (eds). IAU Symp. 101, Supernova Remnants and Their X-ray Emission. Reidel, Dordrecht: Reidel, p. 101
Milne D. K., 1979, Australian J. Phys. 32, 83
Page D., 1997, in: Alpar M. A., Buccheri R., van Paradijs J. (eds). Many Faces of Neutron Stars. Kluwer, Dordrecht, in press
Page D., Shibanov Yu. A., Zavlin V. E., 1996, in: Zimmermann H.-U, Trümper J., Yorke H. (eds). Röntgenstrahlung from Universe. MPE Report 263, p. 173
Pavlov G. G., Shibanov Yu. A., Zavlin V. E., Meyer R. D., 1995, in: Alpar M. A., Kiziloğlu Ü., van Paradijs J. (eds). The Lives of the Neutron Stars. Kluwer, Dordrecht, p. 71
Pavlov G. G., Zavlin V. E., 1997, ApJ 490, L91
Petre R., Becker C. M., Winkler P. F., 1996, ApJ 465, L43
Raymond J. C., Smith B. W., 1977, ApJS 35, 419
Roger R. S., Milne D. K., Kesteven M. J., Wellington K. J., Haynes R. F., 1988, ApJ 332, 940
Shibanov Yu. A., Yakovlev D. G., 1996, A&A 309, 171
Tuohy I. R., Garmire G. P., 1980, ApJ 239, L107
Tuohy I. R., et al., 1979, ApJ 230, L27
Van Riper K. A., Link B., Epstein R. I., 1995, ApJ 448, 294
Vasisht G., Kulkarni S. R., Anderson S. B., Hamilton T. T., Kawai N., 1997, ApJ 476, L43 (V97)
Zavlin V. E., Pavlov G. G., 1998, A&A 329, 583
Zavlin V. E., Pavlov G. G., Shibanov Yu. A., 1996, A&A 315, 141
Zimmermann H.-U., Becker W., Belloni T., et al., 1994, EXSAS Users's Guide. MPE Report 257, ROSAT Scientific Data Center, Garching

This article was processed by the author using Springer-Verlag LaTeX A&A style file *L-AA* version 3.